Studying murine hindlimb ischemia by photoacoustic microscopy

Shuoqi Ye (叶硕奇)[1], Junyu Yang (杨君宇)[2], Jianzhong Xi (席建忠)[2], Qiushi Ren (任秋实)[1,2], and Changhui Li (李长辉)[2*]

[1]*School of Life Science, Shanghai Jiao Tong University, Shanghai 200240, China*

[2]*Department of Biomedical Engineering, Peking University, Beijing 100871, China*

[*]*Corresponding author: chli@pku.edu.cn*

Received May 14, 2012; accepted July 11, 2012; posted online November 30, 2012

The murine model of hindlimb ischemia is extensively used in studies on the physiology and pathology of ischemia and angiogenesis. Traditional non-invasive evaluation methods, such as laser or ultrasound blood flow perfusion imaging and micro-CT angiography, are limited either by low resolution or toxic exogenous agents. Relying on intrinsic high optical absorption contrast, we conduct label-free imaging of subcutaneous blood vasculature in the hindlimb of murine models by photoacoustic microscopy (PAM). The angiogenesis induced by ischemia in the hindlimb is successfully observed at high resolution *in vivo* and non-invasively. PAM is a potentially powerful imaging method for studying ischemic diseases and resultant angiogenesis.

OCIS codes: 170.5810, 170.5120, 170.3880.

doi: 10.3788/COL201210.121701.

Peripheral vascular disease (PVD) imposes a serious effect on human health, affecting 12% to 14% of the general population; up to 20% of those who are more than 70 years old suffer from this disease[1,2]. About 10 million people in the United States suffer from PVD[1], yet effective treatment remains limited[3] given the insufficient understanding of its pathology. The murine model of hindlimb ischemia is one of the most important animal models in the study of ischemic diseases and angiogenesis mechanisms[4,5]. Traditionally, researchers evaluate the models by using laser or ultrasound Doppler perfusion imaging based on flow information[6−8]. However, due to the low spatial resolution or low sensitivity without contrast agent[9,10], using these methods to retrieve subcutaneous vascularity at the single vessel level is challenging. Although computerized tomography angiography enables 3D imaging of the microvascular system at high spatial resolution, it relies on toxic exogenous contrast agents and ionizing radiation, which are unsuitable for studies on chronic diseases. Thus, identifying a novel method that can provide sufficient imaging depth, as well as high-resolution, non-invasive, label-free, and *in vivo* imaging for the study of murine hindlimb ischemia model is necessary.

Photoacoustic tomography (PAT) is an emerging hybrid biomedical imaging method that combines optical contrast with ultrasonic detection[11,12]. It detects the ultrasonic signals generated from a target after absorbing the electromagnetic energy of short laser pulses. Microscopic PAT, or photoacoustic microscopy (PAM), is a scanning imaging modality that enables high-resolution subcutaneous imaging by using focused light or a focused ultrasonic transducer[13,14]. Over the past several years, PAM has been proven superior in imaging subcutaneous vasculature[15−18].

In this letter, we implemented PAM in studying angiogenesis in hindlimb ischemic murine models. Unlike previous research, in which angiogenesis was induced through cancer growth or medical stimulation, we focused on angiogenesis as a consequence of ischemia. Thus, our work is expected to provide additional information on investigating ischemia, wound healing, and tissue regeneration.

The experimental setup of our imaging system is shown in Fig. 1. We employed dark field illumination, in which light forms a donut-shape pattern on the skin surface and obliquely converges into the skin at an incident angle of 45°[14]. The irradiation laser pulses (532 nm) generated by an Nd:YAG laser system (repetition rate: 10 Hz, pulse width: 10 ns) was coupled to a 600-μm multi-mode fiber. An ultrasonic transducer (center frequency: 20 MHz, Olympus V-212-BB-RM) with an acoustic lens (NA: 0.46) attached to its front was used to detect photoacoustic (PA) signals. The ultrasonic signal was amplified by an amplifier (Mini-Circuits ZFL-500) and then recorded with a 14-bit high-speed acquisition card (GAGE CompuScope 14200, sampling rate: 200 MS/s). During the imaging process, a mouse was narcotized with a gas anesthesia system (Matrx). The water tank and the animal were fixed while the imaging head performed 2D scanning without signal averaging. Laser fluence on the skin surface was below 15 mJ/cm^2, which was lower than the safety limit indicated by the American National Standards Institute at 532 nm (20 mJ/cm^2).

The envelope of each A-line raw data was used to generate an image. The lateral and axial resolutions of our imaging system were measured by analyzing the line spread function from the image of a carbon fiber (diameter, less than 10 μm; Fig. 2). According to the full-width at half-maximum (FWHM) of the fitted profile, the lateral and axial resolutions of the system are 100 and 105 μm, respectively. The lateral resolution is determined by the center frequency of the transducer and the NA of the acoustic lens. The axial resolution is determined by the bandwidth of the transducer. Both resolutions can be improved further by using a transducer with a high center frequency.

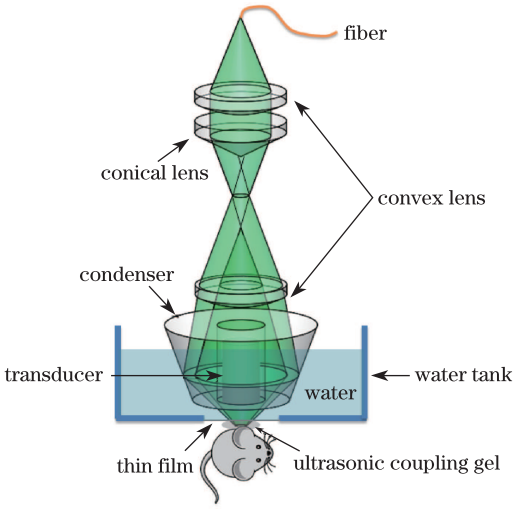

Fig. 1. Experimental setup.

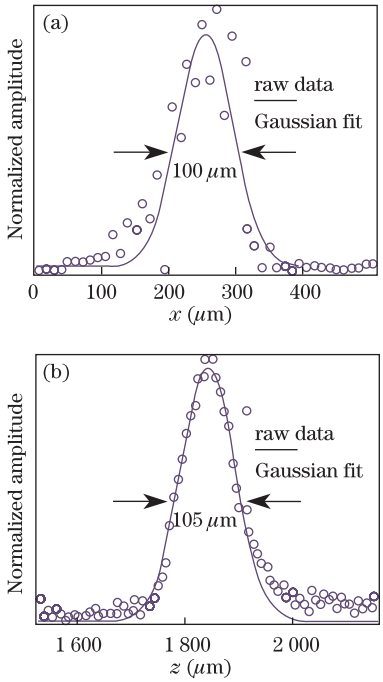

Fig. 2. (a) Lateral and (b) axial profiles of a carbon fiber imaged by PAM.

KM mice that weigh 25–30 g were used in our experiments. The animals were first anesthetized with pentobarbital solution at a proportion of 0.1 mg/g. Then, the hair on the hindlimb was removed using a shaver and hair removal cream. During the experiment, a mouse was fixed on an animal bed under oxygen with 1% isoflurane; the animal was exposed to the oxygen via a homemade breathing mask. In addition, ultrasound gel was applied on the surface of the skin for acoustic coupling. All the experiments complied with the protocols approved by the Institutional Animal Care and Use Committee of Peking University. After the experiments, the mouse was returned to its initial living conditions, and no observable damage due to laser light exposure was found.

We first imaged the subcutaneous blood vasculature in the hindlimb of a healthy mouse. Because femoral vessels lie in a shallow region and are positioned relatively parallel to the skin surface, only PAM maximum amplitude projection images are used. The PAM imaging result and its optical photographic counterpart are shown in Fig. 3. PAM enabled the successful imaging of the large and small vessels of the lower hindlimb at high contrast without exogenous labeling (Fig. 3(a)). Signal-to-noise ratio (SNR) reached up to 40 dB for large and shallow vessels and 10–20 dB for small vessels and those located more deeply in the skin. However, only a few major vessels can be distinguished in Fig. 3(b). These results demonstrate that PAM has a superior advantage in imaging subcutaneous hindlimb vessels.

Another mouse that underwent surgery for femoral artery ligation was used to prepare the hindlimb ischemic model. A 1-cm–long incision was made in the left hindlimb of the mouse by using surgical scissors, and the incision was daubed with PBS-moistened swabs to brush fat tissue away. After this, the femoral artery was located and then ligatured with sutures at two points positioned 2–4 mm apart. Then, the vessel segment between two ligatured points was cut off, and then the incision was closed using Vicryl sutures. The animal was imaged 2 and 20 days after surgery.

The PAM imaging results (20 days after surgery) for the mouse with hindlimb ischemia are shown in Figs. 4(a) and (b). Figures 4(c) and (d) are the images of the left and the right limbs, respectively (the box corresponds to the PAM imaging region). Two obvious black spots caused by ligation in the left limb are shown in the photograph (Fig. 4(c)). Correspondingly, two bright spots (marked by dashed arrows) are present in the PAM image (Fig. 4(a)), indicating strong light absorption by the two black sutures. The PAM image shows that although major vessels break down in the central region, other surrounding vascular structures exist, indicating the bypass of blood circulation. This feature is consistent with the laser Doppler perfusion imaging result in Fig. 4(e) where a "non-flow area" presented in the left hindlimb. Figure 5 compares the size of the vessels between two legs. The vessel ligatured in the left hindlimb was about 200 μm, making it thinner than that in the right hindlimb (about 300 μm). This size difference indicates lower blood flow perfusion as a consequence of ischemia.

In addition to shrinkage in major femoral vessels, angiogenesis was observed through the comparison of the vasculature in the ligatured limb 2 and 20 days after surgery. Figures 6(a) and (b) show the PAM images for the left hindlimb at the same region but at different dates. Blood clots and scars around the incision partially blocked the illumination of the sutures, leading to the absence of two bright spots in Fig. 6(a). Nevertheless, in the areas without blood clots (marked by a dashed box in the figure), angiogenesis was clearly observed. The arrows point to major palingenetic vessels along with the ligatured vessel, which compensates for the hindlimb ischemia.

We successfully obtained high-resolution and high-contrast images of subcutaneous blood vasculature in the hindlimb of murine models *in vivo* and non-invasively. Angiogenesis was observed at superior resolution. This work demonstrates that PAM exhibits promising potential in the study of ischemic diseases and angiogenesis

mechanisms. In addition, spectroscopic PA imaging based on spectral-dependent absorption characteristics enables the mapping of oxygen saturation in the circulatory system[17,19,20], an issue that we will focus on in future work. For imaging speed, scanning a 6-mm-wide and 12-mm-long area (with a step size of 40 μm) was completed within 80–90 min. This limitation was primarily due to the repetition rate of the pulsed laser. Imaging speed can be improved either by using a high-repetition-rate pulsed laser or an ultrasonic transducer array[21].

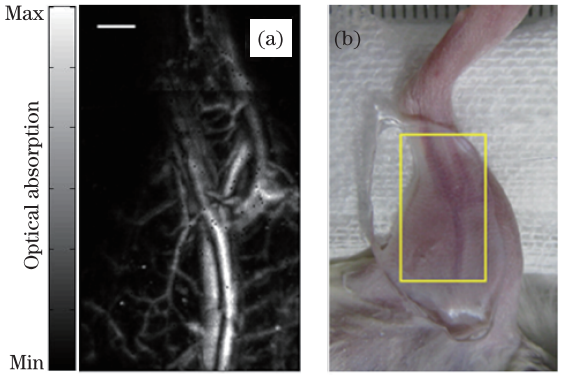

Fig. 3. (a) Maximum amplitude projection imaging of the subcutaneous blood vasculature in the hindlimb of a healthy mouse. Scale bar: 1 mm. (b) Photograph of the hindlimb. Imaging area in (a) is indicated by the rectangle marked in (b).

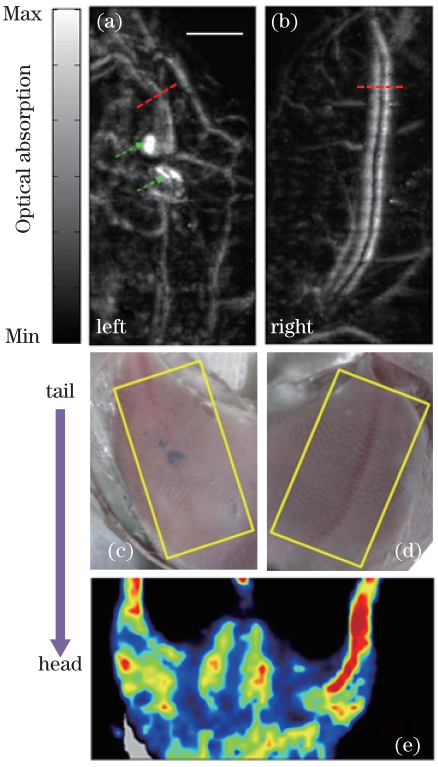

Fig. 4. (Color online) Imaging of mouse with hindlimb ischemia. (a) and (b) PAM imaging results; photographs of the imaging area in the (c) left and (d) right hindlimbs; (e) result of laser Doppler perfusion imaging. Scale bar: 2 mm.

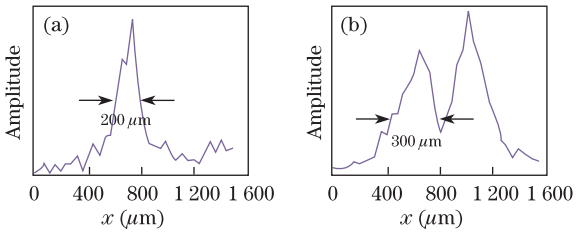

Fig. 5. Comparison of the vessels in the left and right hindlimbs. (a) Cross-section profiles along the red dashed line in Fig. 4(a); (b) cross-section profiles along the red dashed line in Fig. 4(b).

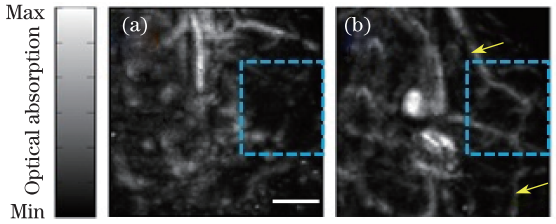

Fig. 6. Comparison of the PAM results for the ligatured limb (a) 2 and (b) 20 days after surgery. Scale bar: 2 mm.

Although PAM enables high-resolution vascular imaging, using it to measure flow information in subcutaneous vessels remains challenging. Thus, PAM can be combined with other imaging modalities, such as ultrasound imaging, laser Doppler perfusion imaging, and CT, to acquire complementary information[22]. We expect this multimodal imaging method to be used in future studies on hindlimb ischemic models.

In conclusion, we present a method for studying ischemic diseases and angiogenesis mechanisms; the method relies on intrinsic optical absorption contrast without labeling. However, PA imaging is by no means exclusive to exogenous contrast agents, such as highly optically absorbing dyes and nanoparticles[23,24]. Labeling vascular endothelial cells is useful because it enables more sensitive observations of angiogenesis even when insufficient red blood cells flow in vessels. Our method can be easily implemented in studying various animal models of hindlimb ischemia, such as those for Wistar rats, SD rats, and Lewis rats, as well as in investigating other vascular system models, such as those for cerebral ischemia.

The first two authors contribute equally to this work. This work was supported by the National Natural Science Foundation of China (No. 61078073) and the National "973" Program of China (No. 2011CB707502).

References

1. M. H. Criqui, Vasc. Med. **6,** 3 (2001).
2. B. A. Golomb, Circulation **114,** 688 (2006).
3. A. T. Hirsch, M. H. Criqui, D. Treat-Jacobson, J. G. Regensteiner, M. A. Creager, J. W. Olin, S. H. Krook, D. B. Hunninghake, A. J. Comerota, M. E. Walsh, M. M. McDermott, and W. R. Hiatt, J. Am. Med. Assoc. **286,** 1317 (2001).

4. H. Niiyama, N. F. Huang, M. D. Rollins, and J. P. Cooke, J. Vis. Exp. **23,** 1035 (2009).
5. M. S. T. Couffinhal, L. P. Zheng, M. Kearney, B. Witzenbishler, and J. M. Isner, Am. J. Patbol. **152,** 6 (1998).
6. H. S. H. Pairleitner, G. Hasenoebrl, and A. Staudacb, Ultrasound Obstet. Gynecol. **14,** 139 (1999).
7. S. K. N. Lassau, P. Opolon, T. De Baere, P. Peronneau, J. Leclere, and A. Roche, Investig. Radiol. **36,** 50 (2001).
8. M. S. A. Fullerton, K.-P. Wilhelm, K. Wådell, C. Anderson, T. Fischer, G. E. Nilsson, and J. Serup, Contact Dermatitis **46,** 129 (2002).
9. J. D. Briers, Physiol. Meas. **22,** R35 (2001).
10. J. C. Miller, H. H. Pien, D. Sahani, A. G. Sorensen, and J. H. Thrall, J. Nat. Cancer Inst. **97,** 172 (2005).
11. C. Li and L. V. Wang, Phys. Med. Bio. **54,** R59 (2009).
12. L. V. Wang and S. Hu, Science **335,** 1458 (2012).
13. K. Maslov, H. F. Zhang, S. Hu, and L. V. Wang, Opt. Lett. **33,** 929 (2008).
14. K. Maslov, G. Stoica, and L. V. Wang, Opt. Lett. **30,** 625 (2005).
15. H. F. Zhang, K. Maslov, M. Li, G. Stoica, and L. V. Wang, Opt. Express **14,** 9317 (2006).
16. E. W. Stein, K. Maslov, and L. V. Wang, J. Appl. Phys. **105,** 102027 (2009).
17. H. F. Zhang, K. Maslov, and L. V. Wang, Nat. Protocols **2,** 797 (2007).
18. C. P. Favazza, L. A. Cornelius, and L. V. Wang, J. Biomed. Opt. **16,** 026004 (2011).
19. H. F. Zhang, K. Maslov, M. Sivaramakrishnan, G. Stoica, and L. V. Wang, Appl. Phys. Lett. **90,** 053901 (2007).
20. H. F. Zhang, K. Maslov, and L. V. Wang, Nat. Protocols **2,** 797 (2007).
21. L. Song, K. Maslov, R. Bitton, K. K. Shung, and L. V. Wang, J. Biomed. Opt. **13,** 054028 (2008).
22. D. R. Reinecke, R. A. Kruger, R. B. Lam, and S. P. Delrio, Proc. SPIE **7564,** 756420 (2010).
23. J. Yao, K. Maslov, S. Hu, and L. V. Wang, J. Biomed. Opt. **14,** 054049 (2009).
24. D. Pan, M. Pramanik, A. Senpan, J. S. Allen, H. Zhang, S. A. Wickline, L. V. Wang, and G. M. Lanza, FASEB J. **25,** 875 (2010).